Available online at www.sciencedirect.com
ScienceDirect
International Journal of Heat and Mass Transfer 50 (2007) 2612–2623
International Journal of HEAT and MASS TRANSFER
www.elsevier.com/locate/ijhmt

Turbulent natural convection in a vertical parallel-plate channel with asymmetric heating

Turgut Yilmaz [a,*], Simon M. Fraser [b]

[a] Istanbul Technical University, Faculty of Mechanical Engineering, Mechanical Engineering Department, Gümüşsuyu, TR-34437, Istanbul, Turkey
[b] University of Strathclyde, Department of Mechanical Engineering, 75 Montrose Street, Glasgow, G1 1XJ, UK

Received 6 October 2005; received in revised form 16 November 2006
Available online 7 February 2007

Abstract

Turbulent natural convection in a vertical parallel plate channel has been investigated both experimentally and numerically. The experimental channel is formed of a uniform temperature heater wall and an opposing glass wall. A fibre flow laser doppler anemometer (LDA) is used to measure velocity profiles along the channel. Simultaneous velocity and temperature profile measurements are made at the channel outlet. A commercial computational fluid dynamics (CFD) code is used to simulate heat transfer and fluid flow in the channel numerically. The code is customised building in some low Reynolds number (LRN) k–ε turbulence models. The numerical method used in this study is found to predict heat transfer and flow rate fairly accurately. It is also capable of capturing velocity and temperature profiles with some accuracy. Experimental and numerical data are presented comparatively in the form of velocity, temperature, and turbulent kinetic energy profiles along the channel for a case. Correlating equations are obtained from the numerical results for heat transfer and induced flow rate and, are presented graphically comparing with other studies available in the literature.

Keywords: Turbulent; Natural; Convection; Vertical; Channel; Experimental

1. Introduction

Natural convection is a preferable heat transfer method wherever possible due to its simplicity, reliability, and cost effectiveness. Natural convection heat transfer and fluid flow in vertical parallel-plate channels are relevant to a wide range of heat exchange applications such as cooling of electronic equipment, solar collectors and passive solar heating and ventilation of buildings, and heat removal in nuclear technology [1–5]. Heat transfer and fluid flow processes of natural convection in vertical parallel-plate channels may take place under laminar or turbulent flow regimes depending on the geometrical size and thermal parameters. Laminar natural convection in vertical parallel-plate channels has been the focus of extensive investigation for many decades due to its wide applicability. It has been studied using experimental, analytical, and numerical techniques [6–11]. The literature covers a wide range of geometrical and thermo-physical aspects of the problem such as the edge effects, interactive convection and radiation, channel aspect ratio, effect of channel wall conductivity, effect of a vent on the channel wall, variable fluid property, and flow reversals [12–23].

Contrary to the extensive research literature on laminar natural convection in vertical parallel-plate channels and considerable amount of research on turbulent natural convection along a single vertical plate [24–29], the number of studies reported on the turbulent natural convection in vertical parallel-plate channels is very limited. The pioneering and most cited experimental work of Miyamoto et al. [30] is an important contribution to the understanding of turbulent natural convection in asymmetrically heated vertical parallel-plate channels. They considered uniform wall heat flux heating mode only and presented correlating equation

* Corresponding author. Tel.: +90 212 2931300x2430; fax: +90 212 2450795; GSM: +90 532 6335300.
E-mail address: yilmaztur@itu.edu.tr (T. Yilmaz).

0017-9310/$ - see front matter © 2007 Elsevier Ltd. All rights reserved.
doi:10.1016/j.ijheatmasstransfer.2006.11.027

Nomenclature

b	channel width
C_μ, $C_{\varepsilon 1}$, $C_{\varepsilon 2}$	LRN k–ε model constants Eqs. (6), (7)
c_p	specific heat (j/kg K)
f_μ, f_1, f_2	LRN k–ε model functions Eqs. (6), (7)
g	gravitational acceleration
G	production of k due to buoyancy Eq. (9)
Gr	Grashof number Eq. (16)
h	heat transfer coefficient (W/m^2 K)
H	channel height (m)
k	turbulent kinetic energy (m^2/s^2)
m	mass flow rate (kg/s)
Nu	average Nusselt number Eq. (18)
p	pressure
p_m	pressure defect
P	production of k due to shearing Eq. (8)
Pr	Prandtl number
q_c	heat convected from the unit area of the heated wall of channel (W/m^2)
Ra	Rayleigh number Eq. (17)
Re	Reynolds number Eq. (15)
Re_t	turbulent Reynolds number Table 1
Re_y	turbulent Reynolds number Table 1
t	time
T	temperature
Tu	turbulence intensity Eq. (13)
u, v	x, y components of velocity
x, y	Cartesian coordinates
y^+	dimensionless coordinate, as given in Table 1
X	dimensionless streamwise direction (x/H)

Greek symbols

β	thermal expansion coefficient
ε	dissipation of turbulent kinetic energy
κ	Von Karman coefficient
λ	thermal conductivity
μ	dynamic viscosity
μ_t	dynamic turbulent viscosity Eq. (7)
ν	kinematic viscosity
ν_t	kinematic turbulent viscosity
ρ	density
σ_t	turbulent Prandtl number
σ_k	Prandtl number of k
σ_ε	Prandtl number of ε

Subscripts

ave	averaged quantity
c	convective or convected, channel, case
exp	experimental value
f	front
h	heated
num	numerical value
w	quantity at the wall
0	quantity at the inlet
∞	ambient quantity, reference quantity
ε	quantity referring to the dissipation of turbulent kinetic energy
k	quantity referring to turbulent kinetic energy
t	quantity referring to turbulence

Superscripts

$'$	fluctuating quantity
–	time averaged quantity

Abbreviations

CFD	computational fluid dynamics
DA	Davidson turbulence model, or numerical results obtained using it
LDA	laser-doppler anemometry
LRN	low Reynolds number
TH	To and Humphrey turbulence model, or numerical results obtained using it
LB	Lam and Bremhorst turbulence model, or numerical results obtained using it

for heat transfer applicable at the fully turbulent region of the channel. Al Azzawi [2] carried out experiments on a similar channel for both uniform wall heat flux and uniform wall temperature and presented correlation for heat transfer. Pederson et al. [4] reported experiments on an asymmetrically heated vertical parallel-plate channel with unheated inlet and insulated outlet sections. They examined high heat fluxes and did not publish experimental data. Fraser et al. [31] reported turbulent natural convection velocity profile measurements in an asymmetrically heated vertical channel. La Pica et al. [32] reported the results of an experimental study on an asymmetrically heated vertical parallel-plate channel with horizontal inlet and outlet. They considered uniform wall heat flux and presented correlations for average Nusselt number, and Reynolds number based on the average inlet velocity and channel width. Cheng and Müller [33] studied turbulent natural convection coupled with radiation in large vertical channels experimentally and numerically. The channel considered had a cross-sectional aspect ratio changing between 0.5 and 1.0 rendering three-dimensionality effects. The heated wall had two emissivity values of 0.4 and 0.9. The channel walls were thermally insulated from the ambient. The most recent experimental study of turbulent natural convection in a vertical flat plate channel was carried out by Habib et al. [34]. They present profiles of vertical component of mean velocity and its rms for only two experimental cases that are conducted for symmetric and asymmetric heating with uniform wall temperature. The asymmetric heating case they had considered was created

by heating one wall 10 °C above the ambient temperature and cooling the opposing wall 10 °C below.

Turbulent natural convection in asymmetrically heated vertical parallel-plate channels has also been the focus of some numerical studies. Sohn [3] carried out an extensive numerical study of turbulent natural convection in asymmetrically heated vertical channel for the uniform wall heat flux heating mode, presenting correlation equations for heat transfer and fluid flow. Fedorov and Viskanta [35] studied turbulent natural convection in a vertical parallel-plate channel numerically, considering both uniform wall heat flux and uniform wall temperature. They presented correlations for average heat transfer and produced scaling relations for induced mass flow rates and average heat transfer.

The literature cited indicates that, however limited, majority of the reported studies on turbulent natural convection in asymmetrically heated vertical parallel-plate channels consider uniform wall heat flux. The only detailed study carried out using uniform wall temperature heating is by Al Azzawi [2]. But, it does not present data regarding turbulent flow field other than mean velocity profiles. There is still a need for experimental data in the literature regarding turbulent flow field characteristics such as velocity, temperature, turbulent kinetic energy, and Reynolds stress profiles in turbulent natural convection along vertical channels. Additional experimental data will be highly valuable in understanding of turbulent natural convection processes in vertical channels and in the validation of numerical techniques.

This paper presents part of a detailed experimental and numerical study on turbulent natural convection of air in an asymmetrically heated vertical parallel-plate channel formed by a uniform wall temperature heated wall and an opposing glass wall [1]. The objective is to contribute to the understanding of turbulent natural convection processes in vertical channels and provide experimental data for the validation of numerical techniques. Velocity and temperature flow field measurements are performed. Turbulent natural convection in the channel is simulated numerically considering three different LRN k–ε turbulence models. For a selected case, experimental and numerical velocity, temperature and turbulent kinetic energy profiles along the channel are presented comparatively, to indicate how the flow develops and how accurately the flow field can be predicted by numerical techniques. Performances of the three LRN k–ε turbulence models used in this study are also compared. Correlations for the induced flow rate and average heat transfer rate are presented.

2. Experimental study

A channel is built to carry out the experimental part of this study. Air velocity and temperature profile measurements were made inside the channel at different elevations. Surface temperatures were also monitored at the channel walls. The channel, instrumentation, experimental procedure, and the uncertainty of experimental data are explained in detail as follows.

2.1. The flow channel

A schematic diagram of the experimental channel used in this study is shown in Fig. 1. The channel is formed by an aluminium heater wall, an opposing glass wall and wooden and perspex sidewalls. The heater wall was designed such that uniform wall temperature boundary condition can be obtained. No direct experimental thermal boundary condition has been planned for the glass front wall. However, it can be heated above the ambient temperature by thermal radiation from the heater wall. Thus, the heater wall needed to be built such that thermal radiation it emits is negligibly low. Therefore, the aluminium plate forming the heater wall surface has been polished carefully so that the surface quality with a very low emissivity, as given in the literature, could be obtained. Thermal radiation calculations were also performed for the system of heater wall, glass (front) wall, and the ambient for the temperature range of the experimental cases of this study. The results indicated that the temperature of the glass wall is raised slightly above the ambient temperature by 2–7 °C depending on the experimental case considered. Preliminary experiments were carried out to validate calculations. The experimental surface temperature data of the glass wall are found to be in close agreement with the calculated values.

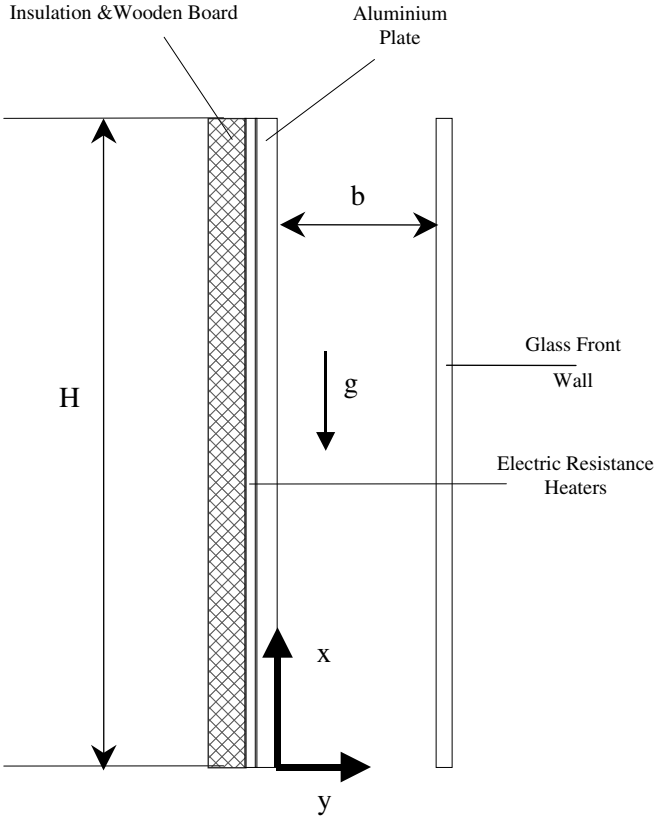

Fig. 1. Schematic diagram of the flow channel.

The heater wall is consisted of 6.35 mm thick, 1 m wide, and 3 m high carefully polished aluminium plate. Nine serpentine shaped graphite heating elements were fitted on the back surface of the aluminium plate and the heating elements were backed with 25 mm thick sheets of ceramic fibre insulation material (Triton Kaowool) which were in turn supported by 19 mm thick plywood boards. A thin sheet of the same insulating material was used to electrically isolate the heating elements from the aluminium plates. The heating elements, each covering area of 0.98 m by 0.3 m were powered via four manual voltage regulators. Three 1.01 m wide, 4 mm thick sheets of plate window glass were held in a metal frame to form the front wall. One transparent side wall was formed by a 8 mm thick 3 m long perspex and the opposite side wall by a 10 mm thick by 3 m long wooden board. Different widths of sidewalls were fabricated for use with each channel width. Teflon coated Cu-Const. thermocouples were fitted on the surface of aluminium plate to monitor wall surface temperature. Thermocouples were located at 0.3 m intervals at the centre-line of the plate and four thermocouples were positioned halfway between the centre-line and the sidewalls at $x = 1$ m and $x = 2$ m heights. Three thermocouples were fitted on to the inner surface of the glass wall at $x = 0.8$ m, 1.8 m and 2.4 m to measure surface temperatures. The channel was mounted on a steel frame that was supported by a frame of scaffolding structure holding the channel inlet at 0.5 m above the floor. The channel assembly was positioned next to one wall of a large laboratory and was surrounded by a 4 m high open-topped hardboard enclosure leaving more than 1 m gap around the channel. A door on one side of the enclosure provided access. The main purpose of the enclosure was to reduce effects of external draughts and to comply with the laser safety regulations.

2.2. Instrumentation

A DANTEC two component fibre flow LDA system was used for the velocity measurements. The system comprised an Ar-Ion laser source, transmission optics, a remote probe, 20 m long fibre-optic cable, and two DANTEC 57 N 10 burst spectrum analysers along with data acquisition and control software. In this study, silicone oil is used as seeding substance. A seeding generator producing an aerosol of silicon oil with an average particle size of 5 μm was used. The slip velocities resulting for this particle size were calculated to be less than 2 mm/s that is negligible for the flow under consideration. The silicon oil aerosol from the seeding generator is fed into a 1 m long 30 mm diameter perspex tube with closed ends. Holes of 2 mm are drilled in this tube to create seeding jets. The tube is placed on the floor beneath the channel. Velocities along the axis of the seeding jets are measured and found to be below 50 mm/s. The flow is continuously seeded since the seeding jets placed 0.5 m below the channel inlet were judged not to influence flow compared to any unavoidable draughts in and around the enclosure.

A temperature data acquisition system was designed, built and used for the measurement of air temperature inside the channel. The system consisted of a temperature probe, data acquisition board, a signal conditioning unit and a host computer. The temperature probe was fabricated by sliding a pair of 25 μm diameter Cromel-Alumel thermocouple wires into a 300 mm long 0.5 mm diameter steel tube. The wires were butt jointed on one end to form the bead and connected to a K type plug fixed on the other end of the tube. The exposed length of thermocouple wire is 5 mm long and epoxy resin is used to fix the wires at the end of the tube. A signal conditioning unit for the thermocouple signal was manufactured. The signal is first linearised and pre-amplified by an AD 595 K type thermocouple amplifier with cold junction compensation. The signal is then fed into the second amplification circuitry that allows the signal to be amplified to the input range of the data acquisition board. Before the temperature signal is connected to the data acquisition board, it was first low-pass filtered with 100 Hz cut-off frequency and then the 50 Hz component was removed by a notch filter to eliminate the noise from the mains electrical supply. The temperature probe was connected to the signal conditioning unit by a 5 m long twisted-pair thick thermocouple wire of the same type as used for the probe. The data acquisition board has 12 bit analogue to digital, digital to analogue (AD/DA) conversion capability along with some other functions. The board was used in monopolar mode so that the highest resolution could be exploited. A Turbo Pascal programme was developed for air temperature data acquisition. The sampling rate used for temperature data acquisition is 100 Hz. The synchronisation of the temperature and velocity were achieved via a connection between the clock-reset line of the BSA synchronisation bus and temperature data acquisition system. When the reset signal from the BSA is detected, the programme starts temperature reading. Surface temperature thermocouples were connected to a temperature measurement device (CIL TA 880) via a manual multiplexer. The device has a resolution of 0.1 °C and allows direct temperature reading for different type of thermocouples. End to end calibrations were performed for both the air temperature probe and surface temperature thermocouples with respect to ice point and the boiling point of water.

Separate traversing mechanisms were used to traverse the velocity and temperature probes. A two-dimensional computer controlled traversing mechanism is used to traverse the optical probe across the channel. The traversing mechanism was located on a platform. To position the optical probe in vertical measurement locations the platform was mounted on a 4 m high pillar structure of scaffolding tubes incorporating sliding supports such that it could be moved vertically. The platform could thus be located and firmly clamped at the desired vertical location. The cross-channel traversing was controlled from the data acquisition card used for the temperature probe. The traversing mechanism had a minimum movement of 10 μm.

The DANTEC 57G15 traversing mechanism was used for temperature probe traversing.

A close circuit TV system was used to view the traversing of the probes. The camera was mounted on the velocity probe traversing mechanism in-line with the laser beam so that the position of probes could be viewed while traversing the probes. The monitor was in the room where the LDA system and computers were accommodated.

2.3. The experiments and experimental procedure

The heater plate power supply was switched on and the surface temperatures, ambient temperature were monitored. It took approximately 2–3 h for the temperatures to stabilise and steady state conditions to be achieved. Approximate voltage levels for each heater group were determined for different wall temperatures by trial and error. Over the surface of the heated wall, the prescribed uniform temperature could be maintained within ±2 °C. Beam separation size of the optical probe prevented measurements being made at the centre-line of the channel. Measurements were made 100 mm away from the centre-line. The laser beams could not be set exactly parallel to the surface. The probe required to be tilted by approximately 6–8° with respect to the wall. Corrections to velocity readings were made through software to account for the effect of tilt angle. In order to set the traversing position the probe was traversed to the wall, (heated or front wall), far enough to eliminate backlash and then moved away from the wall while observing the signal on the oscilloscope. When the centre of the optical probe volume is at the surface of the wall, the signal on the oscilloscope is that of the optical noise due to reflection from the wall. The probe was traversed very slowly away from the wall toward the centre of the channel monitoring the signal on the oscilloscope. When the amplitude of the signal (noise) was a maximum, the position was assumed to be the wall surface. From that position the probe was moved to the first measurement location. The temperature probe was located 1 mm above the optical measuring volume. To set the position, at the first measurement location, the thermocouple bead was submerged into the optical probe volume that gave a sudden rise of temperature due to heating by the laser beam. When this condition was obtained the temperature probe was raised back 1 mm above the optical probe before any reading was taken. The procedure was repeated for both walls. Making a profile reading across the channel took 4–6 h. Surface temperatures were monitored throughout the experiments and small adjustments were made in order to maintain the prescribed surface temperature. The measurements were carried out for a specified set of parameters under the same ambient conditions as closely as possible.

2.4. Uncertainty of the experimental data

An uncertainty analysis is carried out to determine the level uncertainty the measurements. Typical uncertainties are calculated to be 0.022 m/s for the mean velocity, 0.2 °C for the flow temperature, 0.9 °C for the surface temperature. Typical relative error for heat transfer and induced mass flow rate are 10.0% and 7.0%, respectively. Details of uncertainty analysis are given in Ref. [1].

3. Numerical study

Turbulent natural convection heat transfer and fluid flow inside the channel considered in this study have been simulated using the finite volume based commercial CFD code PHOENICS, version 1.66. The code is customised building in some LRN k–ε turbulence models. The models employed in this study are Lam and Bremhorst LRN k–ε Model (LB) [36], To and Humphrey LRN k–ε Model (TH) [37] and Davidson LRN k–ε Model (DA) [38,39]. The models of TH and DA were developed considering natural convection flows whereas the LB model was developed for forced convection flows.

3.1. Modelling assumptions and problem formulation

The flow through the channel, shown in Fig. 1, is induced entirely by buoyancy. One wall of the channel is maintained at a uniform constant temperature while the opposing wall is kept adiabatic. Air is drawn into the channel at the inlet under the ambient conditions of P_∞, T_∞, ρ_∞, and the heated fluid is discharged into the ambient at the outlet. The ambient is quiescent, thus no thermal mixing of inlet and outlet of the channel takes place. All transport processes take place at steady state and are two-dimensional. The fluid is air with $Pr = 0.7$. The properties of air are constant except density. The density changes only with temperature and obeys the ideal gas law. Thermal radiation is neglected. The flow within the entire channel is turbulent. It is expected that the flow will start as laminar in the inlet region of the channel undergoing transition and becoming fully turbulent downstream, depending upon the thermal and geometric parameters. The completely turbulent flow assumption, however, appears sensible due to the lack of transition criteria. The measurements made in this study suggest some level of turbulence at the channel inlet. The time averaged continuity, momentum and energy equations along with turbulence model equations can be written as follows.

Continuity equation

$$\frac{\partial(\bar{\rho}\bar{u})}{\partial x} + \frac{\partial(\bar{\rho}\bar{v})}{\partial y} = 0 \tag{1}$$

x component of momentum equation

$$(\bar{\rho}\bar{u})\frac{\partial \bar{u}}{\partial x} + (\bar{\rho}\bar{v})\frac{\partial \bar{u}}{\partial y} = -\frac{\partial \bar{p}_m}{\partial x} + (\bar{\rho} - \rho_\infty)g + \frac{\partial}{\partial x}\left[(\mu + \mu_t)\frac{\partial \bar{u}}{\partial x}\right] + \frac{\partial}{\partial y}\left[(\mu + \mu_t)\frac{\partial \bar{u}}{\partial y}\right] \tag{2}$$

y component of momentum equation

$$(\bar{\rho}\bar{u})\frac{\partial \bar{v}}{\partial x}+(\bar{\rho}\bar{v})\frac{\partial \bar{v}}{\partial y}=-\frac{\partial \bar{p}_m}{\partial y}+\frac{\partial}{\partial x}\left[(\mu+\mu_t)\frac{\partial \bar{v}}{\partial x}\right]+\frac{\partial}{\partial y}\left[(\mu+\mu_t)\frac{\partial \bar{v}}{\partial y}\right] \tag{3}$$

In Eqs. (2) and (3), $\bar{p}_m$ is pressure defect defined as $\bar{p}_m=\bar{p}-p_\infty$, which has been commonly used by previous investigators [8,15,21]. In this definition, $\bar{p}$ is the pressure of fluid at a point inside the channel, and p_∞ is pressure of the fluid at the same point in the channel if the temperature were uniform at the ambient temperature, T_∞, within the entire channel.

Energy equation

$$c_p(\bar{\rho}\bar{u})\frac{\partial \bar{T}}{\partial x}+c_p(\bar{\rho}\bar{v})\frac{\partial \bar{T}}{\partial y}=\frac{\partial}{\partial x}\left[(\lambda+\frac{c_p\mu_t}{\sigma_t})\frac{\partial \bar{T}}{\partial x}\right]+\frac{\partial}{\partial y}\left[(\lambda+\frac{c_p\mu_t}{\sigma_t})\frac{\partial \bar{T}}{\partial y}\right] \tag{4}$$

LRN k–ε turbulence model equations

$$(\bar{\rho}\bar{u})\frac{\partial k}{\partial x}+(\bar{\rho}\bar{v})\frac{\partial k}{\partial y}=\frac{\partial}{\partial x}\left[(\mu+\frac{\mu_t}{\sigma_k})\frac{\partial k}{\partial x}\right]+\frac{\partial}{\partial y}\left[(\mu+\frac{\mu_t}{\sigma_k})\frac{\partial k}{\partial y}\right]+(P+G-\bar{\rho}\varepsilon) \tag{5}$$

$$(\bar{\rho}\bar{u})\frac{\partial \varepsilon}{\partial x}+(\bar{\rho}\bar{v})\frac{\partial \varepsilon}{\partial y}=\frac{\partial}{\partial x}\left[(\mu+\frac{\mu_t}{\sigma_k})\frac{\partial \varepsilon}{\partial x}\right]+\frac{\partial}{\partial y}\left[(\mu+\frac{\mu_t}{\sigma_k})\frac{\partial \varepsilon}{\partial y}\right]+\frac{\varepsilon}{k}(C_{\varepsilon1}f_1P+C_{\varepsilon1}G-C_{\varepsilon2}f_2\bar{\rho}\varepsilon) \tag{6}$$

where

$$\mu_t=\bar{\rho}C_\mu f_\mu\frac{k^2}{\varepsilon} \tag{7}$$

$$P=\mu_t\left\{2\left[\left(\frac{\partial \bar{u}}{\partial x}\right)^2+\left(\frac{\partial \bar{v}}{\partial y}\right)^2\right]+\left(\frac{\partial \bar{u}}{\partial y}+\frac{\partial \bar{v}}{\partial x}\right)^2\right\} \tag{8}$$

$$G=\beta\frac{\mu_t}{\sigma_t}\frac{\partial \overline{T}}{\partial x}g \tag{9}$$

In the above equations μ_t is turbulent dynamic viscosity, P and G are the production of turbulent kinetic energy due to shearing and buoyancy respectively. C_μ, $C_{\varepsilon1}$, and $C_{\varepsilon2}$, are model constants and σ_t, σ_k, σ_ε are turbulent Prandtl number defined for the relevant variable. The values of the model constants for all models considered are $C_\mu=0.09$, $C_{\varepsilon1}=1.44$, $C_{\varepsilon2}=1.44$, $\sigma_t=0.9$, $\sigma_k=1.0$, $\sigma_\varepsilon=1.3$. f_μ, f_1, f_2 are the LRN k–ε turbulence model functions to account for the wall damping. The definitions of the model functions depend on the model employed and are given in Table 1 along with the wall boundary conditions of ε for the turbulence models considered in this study.

3.2. Boundary conditions

At the channel inlet, the ambient fluid accelerates from rest to the induced velocity, u_0, as the fluid inside the channel rises due to heating. Since the ambient is quiescent, there exists a pressure defect, $\bar{p}_m$, to account for this effect. The boundary conditions used at the inlet for velocity and pressure are given in Eq. (10). However, u_0 is not known prior to the solutions. It is obtained, along with the values of other variables in the flow field, from solution of the governing equations applying the boundary conditions set out in the following:

$$\bar{v}=0,\quad \bar{u}=\bar{u}_0,\quad \bar{p}_{m_0}=-\frac{1}{2}\bar{\rho}_0\bar{u}_0^2 \tag{10}$$

Temperature of the incoming air at the inlet is set equal to the ambient temperature. The values of k and ε at the inlet are calculated from Eqs. (11) and (12).

$$k_0=\frac{3}{2}(Tu_0)^2(\bar{u}_{0,\mathrm{ave}})^2 \tag{11}$$

$$\varepsilon=\varepsilon_0=C_\mu^{3/4}\frac{k_0^{3/2}}{\kappa b} \tag{12}$$

where Tu_0 is the turbulent intensity at the inlet and given by,

$$Tu_0=\left(\frac{u'^2+v'^2+w'^2}{3}\right)^{1/2}\Big/(\bar{u}_{0,\mathrm{ave}}) \tag{13}$$

κ is the Karman coefficient and its value is 0.41.

At the outlet of the channel, the pressure defect is equal to zero as given in Eq. (14).

$$\bar{p}_m=0 \tag{14}$$

At the walls no-slip boundary condition is applied for velocity and the values of k is set to zero. The boundary condition of ε at the wall is taken as it is listed in Table 1 for the respective turbulence model. The prescribed uniform temperature is used as thermal boundary condition

Table 1
Functions of the low Reynolds number k–ε turbulence models

Model	f_μ	f_1	f_2	ε_w
LB	$(1.0-\exp(-0.0165Re_y))^2\left(1.0+\frac{20.5}{Re_t}\right)$	$1.0+\left(\frac{0.05}{f_\mu}\right)^3$	$(1.0-\exp[-Re_t^2])$	$\frac{\partial \varepsilon}{\partial y}=0$
TH	$\exp\left(\frac{-2.5}{1.0+0.02Re_t}\right)$	1.0	$(1.0-0.3\exp[-Re_t^2])f_3$ for $y^+\geqslant 5f_3=1$ for $y^+<5f_3=1.0-\exp(-Re_t^2)$	$2\nu\left(\frac{\partial k^{0.5}}{\partial y}\right)^2$
DA	$\exp\left(\frac{-3.4}{1.0+0.02Re_t}\right)$	$1+\left(\frac{0.14}{f_\mu}\right)^3$	$(1.0-0.27\exp[-Re_t^2])(1-\exp[-Re_y])$	$\frac{\partial \varepsilon}{\partial y}=0$

$$Re_t=\frac{k^2}{\nu\varepsilon},\quad Re_y=\frac{y\sqrt{k}}{\nu},\quad y^+=y/\nu(\partial u/\partial y)$$

at the heated wall with molecular diffusion transport. The molecular transport approach is implemented by selecting the sizes of the first one or two cells of the computational domain such that they remain in the viscous sub-layer that is proposed by George and Cap [29].

3.3. Numerical algorithm, solution technique and the solutions

A customised form of the commercial CFD code PHOENICS version 1.66 is used in this study to carry out numerical analysis. PHOENICS iteratively solves linear algebraic equations resulting from finite volume discretisation of the governing partial differential equations. The unknown pressure field poses a difficulty in the numerical solution of the momentum equations to produce velocity components. There is no equation for the pressure, unlike the velocity, energy, etc., that it can be calculated from. The pressure correction process along with the solution procedure is known as the SIMPLE algorithm [40]. Patankar [40] explains a revised form of it, the SIMPLER algorithm. However, PHOENICS uses another variant called SIMPLEST [41]. The hybrid scheme is used for the discretisation of convective-diffusive transport. The staggered grid approach was taken for the discretisation of momentum equations. The overall procedure regarding numerical algorithm and the solution technique are explained by Spalding [42,43], and Ludwig et al. [43] in detail. Preliminary computations were carried out to determine the best grid size, grid pattern, and convenient values of the solution control parameters.

One of the uniform wall temperature experimental cases, the case with $T_w = 100\ ^\circ C$ and $b/H = 1/30$, of Ref. [1] was chosen as the test case. The average of the turbulent kinetic energy measured at the first elevation was used as a uniform boundary condition for the test cases. A grid sensitivity analysis of the numerical solutions has been carried out considering all three LRN k–ε turbulence models, comparing heat transfer and induced mass flow rates with experimental results. Sensitivity of the solutions to the grid pattern and grid size in the streamwise direction was negligibly low for all three models. In the cross-stream direction, however, the model of DA was found to be sensitive to the number of grids and grid pattern, requiring finer grid near the walls. It produced heat transfer results that differed by as much as 13% and flow rate results by almost 4% for coarser grids. Both heat transfer and mass flow rate result discrepancies for the other two models were within a band 2% for the same range of grid pattern and size. Different grid sizes and grid patterns were selected for each LRN k–ε turbulence model. Convergence to a solution was determined by checking overall balances of mass and energy. When the inflow and outflow mass flow rates were equal within a limit and the overall balance of energy was satisfied, the run was assumed to have converged. All of the cases were run to converge to the same level of residuals. Details of grid dependency analysis and convergence criteria are given in Ref. [1]. The effect of turbulent kinetic energy boundary condition at the inlet is also investigated. For this purpose, calculations are made applying a uniform k at the inlet as 0.5 and 0.25 multiples of the measured average. A variable k at the inlet is also considered by applying the measured profile of k at the first elevation as the inlet boundary condition. Although not presented here, the results indicate a considerable sensitivity of heat transfer and induced flow rate by a reduction of almost 10% in the estimated heat transfer [1].

Final calculations were made for all the experimental cases and additional cases outside the experimental range. The average of the turbulent kinetic energy measured at the first elevation was used as a uniform boundary condition for all the numerical cases corresponding to the relevant experimental case. The numerical cases outside the experimental range, however, are run applying 10% turbulence intensity at the inlet. This is assumed to be reasonable approach as measured turbulence intensity at the inlet for the test case is 13%. The value of turbulent kinetic energy at the inlet for these cases is calculated using Eq. (11). The value of $\bar{u}_{0,ave}$ which is used in Eq. (11) to compute the inlet value for turbulent kinetic energy is determined from the empirical correlation given in Eq. (19). The constants for this correlation are listed in Table 3.

4. Results and discussion

Velocity profile measurements across the channel for five cases are carried out at five different elevations along the channel. At the highest elevation, nearest to the outlet, both velocity and temperature were measured simultaneously. For the experimental cases, the channel width is set to 0.1 m. The wall temperatures are set to the values of 60, 75, 90, 100 and 130 °C in turn. For the case with 130 °C wall temperature, the channel with is set to 0.15 m and velocity profile measurement is made at the first elevation near the inlet. This has provided a wide enough range for the correlation of induced flow rate from the experimental data. Turbulent kinetic energy profiles are also created for all the velocity profile elevations. Average heat transfer from the channel and induced mass flow rates are calculated from the experimental data. Numerical calculations are made for all the experimental cases and additional cases outside the range of the experimental cases. The $Ra(b/H)$ range covered by numerical calculations changed between 5944 and 856,196. The results of experimental and numerical study are presented below comparatively. The inner surface temperature of the glass wall has been measured at three vertical locations during the experiments and presented in graphical form.

4.1. Heat transfer and induced flow rate

The experimental and numerical heat transfer and induced flow rate data are presented in Table 2 for all the cases and turbulence models considered. Numerical results are listed as divided by experimental values. Considering

Table 2
Comparison of experimental and numerical heat transfer and flow rate

T_w (°C)	Experimental		LB		TH		DA	
	$q_{c,exp}$ (W/m^2)	m_{exp} (gr/s)	$\frac{q_{c,num}}{q_{c,exp}}$	$\frac{m_{num}}{m_{exp}}$	$\frac{q_{c,num}}{q_{c,exp}}$	$\frac{m_{num}}{m_{exp}}$	$\frac{q_{c,num}}{q_{c,exp}}$	$\frac{m_{num}}{m_{exp}}$
60	144.8	59.87	0.95	1.12	1.18	1.10	1.03	1.10
75	219.2	67.38	0.94	1.13	1.17	1.12	1.02	1.12
90	304.6	79.20	0.92	1.06	1.15	1.05	1.00	1.05
100	360.3	85.41	0.92	1.07	1.16	1.04	1.00	1.03
130	553.1	106.17	0.90	0.97	1.14	0.97	0.98	0.96

relative errors of 10.0% and 7.0% for heat transfer and mass flow rate respectively. Table 2 indicates that the numerical technique performs well in predicting heat transfer and induced flow rate. The LB LRN k–ε Model underestimates heat transfer by as much as 10% of the experimental value while overestimating induced flow rate by up to 13%. The TH model on the other hand, over estimates heat transfer by as much as 18% and induced flow rate by up to 12%. The DA model performed similar to the other models as far as flow rate is concerned. However, it predicted heat transfer within a limit of ±3% of the experiments. In all models mass flow rate is over estimated for all experimental cases except at the highest wall temperature case where all models under estimate. The heat flux from the heater wall due to thermal radiation was calculated and compared with the experimental convective heat flux from the channel. It was found equal or less than 7% of the convective flux for all experimental cases, which is below the experimental heat flux uncertainty of 10%. Thus neglecting of thermal radiation in the simulations is justified.

4.2. Surface temperature distribution on the glass wall

Temperature distribution at the inner surface of the glass wall has been measured during the experiments. The measurements were made at three vertical locations, $x = 0.8$ m, 1.8 m and 2.4 m. The results are presented in Fig. 2 graphically for five cases. They indicate that glass wall is slightly heated above the ambient temperature which was between 22 °C and 23 °C for all the cases. The average of the measured wall temperature has been calculated. It changes between 2.1 and 5.0 °C depending on the experimental case, the lower value pertaining to the case with the lowest heater wall temperature. They are also in good agreement with previously mentioned calculated wall temperature range of 2.0–7.0 °C considering thermal radiation.

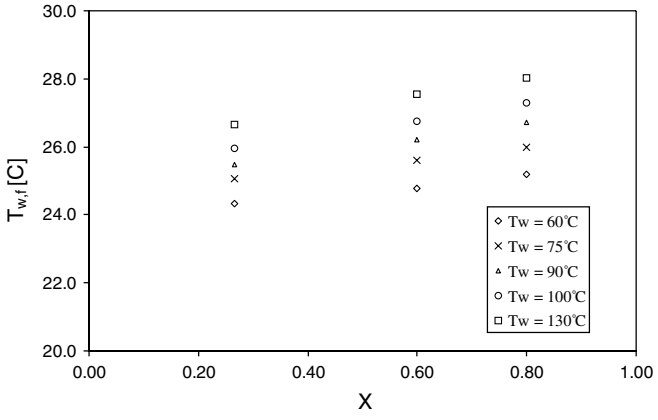

Fig. 2. Experimental temperature distribution at the inner surface of the glass wall.

4.3. Velocity, temperature and turbulent kinetic energy profiles

The natural convection flow along a vertical channel similar to that of the present study is expected to start laminar at the inlet in the absence of any disturbance, undergo transition and finally become fully turbulent near the outlet depending upon the geometrical size and thermal parameters. In the present study, no measure has been taken to minimise possible disturbances that may be introduced to the flow at the inlet edges of the experimental channel. Experimental velocity profiles for the case with $T_w = 100$ °C are presented in Figs. 3–5 comparatively with numerical velocity profiles obtained for all three LRN k–ε models. In order to avoid ambiguity, the profiles of each turbulence model are given on a separate diagram. Experimental velocity profiles in the figures indicate that the flow starts almost uniform near the channel inlet with only a

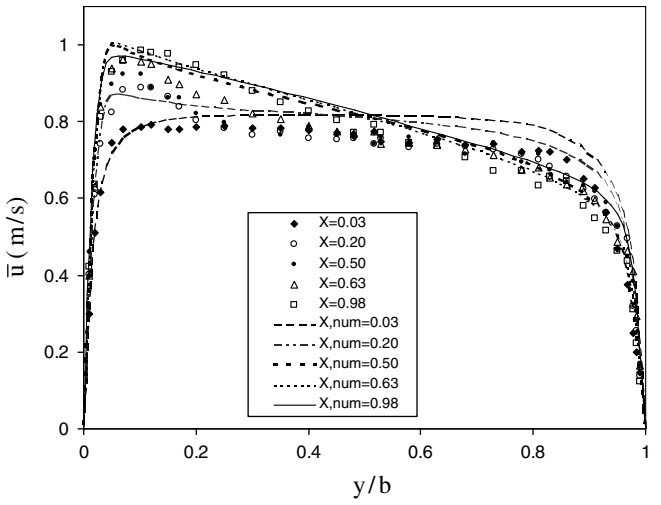

Fig. 3. Experimental and numerical velocity profiles, $T_w = 100$ °C, LB model.

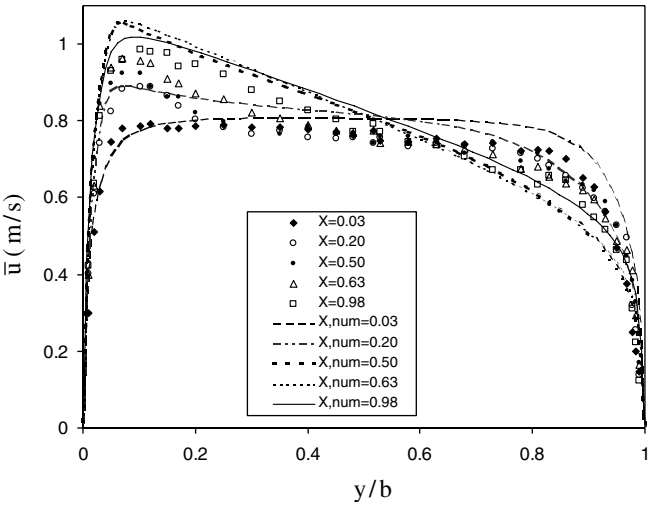

Fig. 4. Experimental and numerical velocity profiles, $T_w = 100\,^{\circ}C$, TH model.

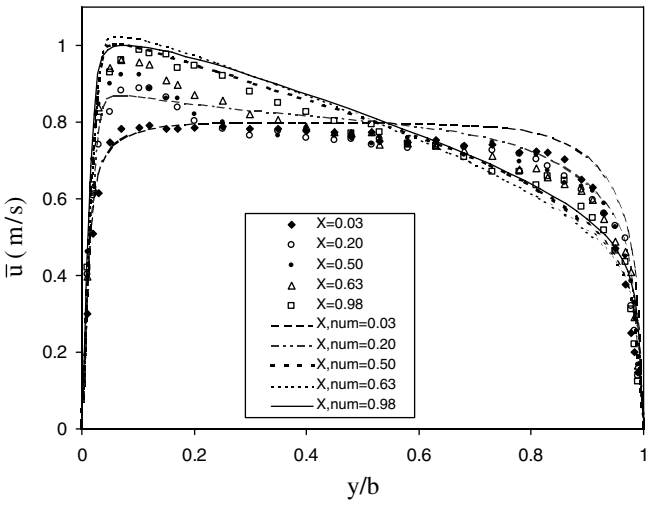

Fig. 5. Experimental and numerical velocity profiles, $T_w = 100\,^{\circ}C$, DA model.

slight distortion towards the heated wall. Downstream through the channel a clear velocity peak develops near the heated wall. The peak is most obvious in the three intermediate profiles. Near the channel exit, the velocity peak weakens and the profile becomes smoother indicating diffusion of momentum across the channel towards the front wall. The profiles bear the hallmarks of a developing flow. The numerical velocity profiles obtained using three LRN k–ε models follow up the experimental profiles to some degree of accuracy, the profiles near the inlet and outlet are best captured. All three models fail to capture the peak near the wall well enough, but develop peaks consistent with the experimental profiles, more emphasised by the models of TH and LB. Another important feature of the numerical profiles is that the profiles at $X = 0.5$ and $X = 0.63$ develop peaks with velocities higher than the experimental values. This is consistent with the results given in Fig. 6 of Ref. [35]. The models of TH and DA produce steeper velocity profiles in the middle to upper half of the channel, especially for $X = 0.5$ and $X = 0.63$. In all, TH and DA models are better in capturing the flow development along the channel compared to LB model. TH model predicts slightly higher values of velocity. The DA model, however, predicts the velocity better overall and best at the uppermost elevation.

Non-dimensionalised temperature profiles near the outlet of the channel for the same case as for the velocity profiles are shown in Fig. 6. The experimental temperature profile has essentially zero gradient at the glass wall. The air temperature profile for the other experimental cases near the channel outlet, however not presented here, also exhibit the same character. Although there are no temperature profile measurements upstream, the profiles near the channel outlet have zero gradients at the glass wall. Considering the values and downstream trend of experimental surface temperature data of the glass wall, Fig. 2, similar profiles may also be expected at the upstream locations as well. Under the circumstances, considering the front (glass) wall as adiabatic in the simulations is justified very well. TH model predicts temperature very well near the heated wall, though it over-predicts the values in the rest of the channel. The other two models, LB and DA, underestimate the temperatures near the heated wall while predicting very well in the remaining of the channel.

In the calculation of turbulent kinetic energy, the z direction component has been taken as equal to the y direction component since there has not been any velocity measurement in z direction. Although this may have resulted in slightly higher values of k since the magnitude of velocity fluctuations in this direction are expected smaller than those in the other directions; this can still be considered a reasonable approach. The averages of x and y direction components of turbulent kinetic energy across the channel width has been calculated from the experimental data. The ratio of cross component to streamwise component are calculated to be 0.55, 0.38, 0.15, 0.17 and 0.23 for the five profile measurement locations of $X = 0.033$, $X = 0.2$, $X = 0.5$, $X = 0.63$ and $X = 0.983$, respectively. The values indicate

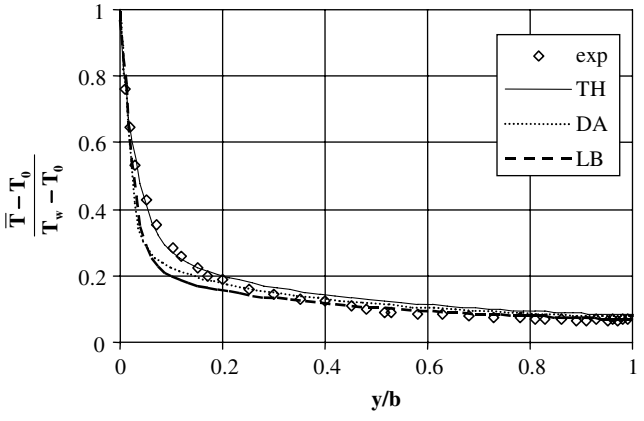

Fig. 6. Experimental and numerical temperature profiles at exit, $T_w = 100\,^{\circ}C$.

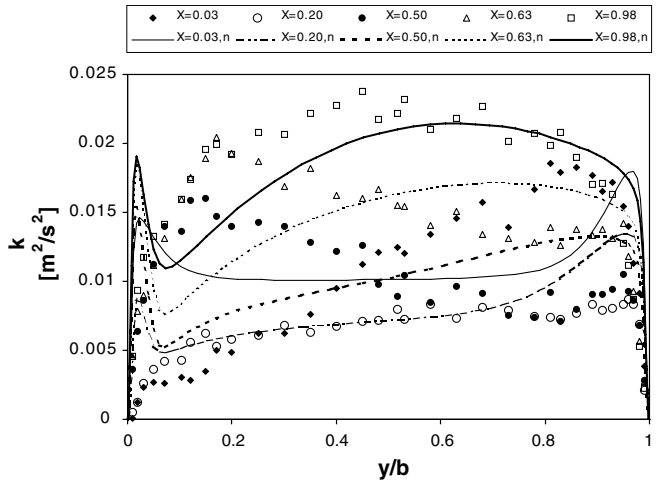

Fig. 7. Turbulent kinetic energy profiles, $T_w = 100\,^{\circ}C$, TH model.

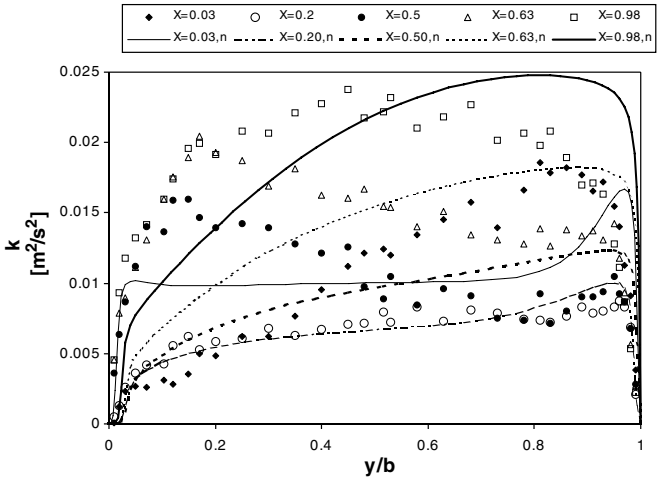

Fig. 8. Turbulent kinetic energy profiles, $T_w = 100\,^{\circ}C$, DA model.

that velocity fluctuations in cross-stream direction are considerably large near the channel inlet. However, they appear to reduce downstream until the mid-height of the channel and then start to increase downstream. Experimental and numerical profiles of turbulent kinetic energy are presented in Figs. 7 and 8 for the TH and DA models, respectively. Although not given here, the model of LB produced similar results to DA model. Experimental turbulent kinetic energy profile at the first elevation is in a magnitude comparable to that at the mid-height of the channel, but skewed towards front wall. At the second elevation, $X = 0.2$ the profile becomes almost uniform and it is reduced in magnitude suggesting laminarisation. At the mid-height, $X = 0.5$, the profile is almost mirror image of that at $X = 0.03$. At the uppermost elevation, turbulent kinetic energy profile becomes almost symmetric resembling to that of developed turbulence, with an increased magnitude compared to the other profiles. Both of the models fail to capture turbulent kinetic energy profiles, except for the elevation of $X = 0.2$. Overall, TH LRN k–ε model performs better, especially at the uppermost elevation.

4.4. Correlating equations for heat transfer and induced flow rates

The dimensionless parameters used in presentation of the numerical and experimental results are defined as follows. Dimensionless numbers of Reynolds, Grashof, Rayleigh and Nusselt are given by Eqs. (15)–(18).

$$Re = \frac{\bar{u}_{0,\mathrm{ave}} b}{\nu} \tag{15}$$

$$Gr = \frac{g\beta(T_{\mathrm{w,h}} - T_0)b^3}{\nu^2} \tag{16}$$

$$Ra = GrPr \tag{17}$$

$$Nu = \frac{q_c b}{(T_{\mathrm{w,h}} - T_0)\lambda} = \frac{hb}{\lambda} \tag{18}$$

Correlating equations were obtained for the average dimensionless heat transfer and induced mass flow rates in the form of Eqs. (19) and (20) from the experimental and numerical results. The constants of equations are listed in Table 3.

$$Re/Gr = n(Ra(b/H))^{\mathrm{p}} \tag{19}$$

$$Nu = m(Ra(b/H))^{\mathrm{c}} \tag{20}$$

Induced flow rate correlations are presented graphically in Fig. 9. As seen from the figure, both numerical and experimental values collapse almost on the same line. Induced flow rate correlation given in Ref. [35] is also plotted on the same diagram. It correlates numerical solution with zero turbulence intensity at the channel inlet. At lower

Table 3
Constants of the correlation equations for induced flow rate and average heat transfer

Model/Exp.	n	P	m	C
Exp.	0.36	−0.54	N/A	N/A
Al Azzawi [2]	N/A	N/A	0.63	0.26
TH	0.47	−0.56	1.01	0.24
DA	0.48	−0.56	0.56	0.28

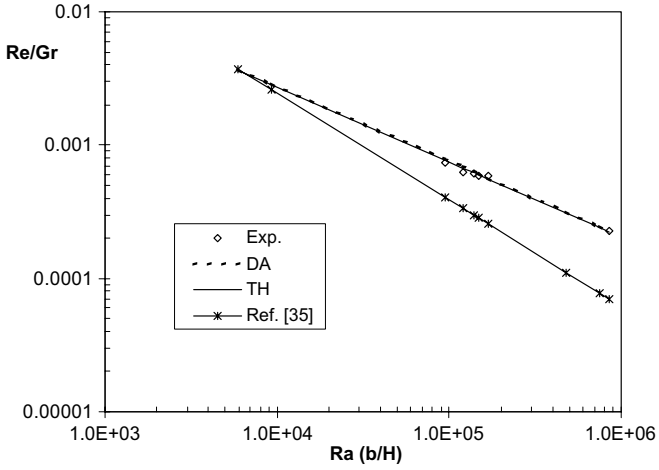

Fig. 9. Dimensionless induced flow rate as function of $Ra(b/H)$.

range of $Ra(b/H)$, the numerical Re/Gr graphs of the current study intersect with the graph produced from the correlation given by Ref. [35] somewhere between the values of 6500 and 7500 of $Ra(b/h)$. This may imply change of flow from laminar to turbulent within this range of $Ra(b/h)$. However, this is just an implication rather than a proven fact. Furthermore, the authors neither have experimental data in that range, nor they came across with any criterion or experimental data in the literature, except the experimental study by Al Azzawi [2], regarding the range of $Ra(b/h)$ for transition from laminar to turbulent of natural convection channel flow under consideration to unquestionably substantiate or disprove the abovementioned implication. Actually, the good agreement of experimental results by Al Azzawi [2] and the results of the numerical solutions of the present study using the turbulence model by Davidson [38,39] given in Fig. 10 considering heat transfer weakens the implication of flow regime change.

The correlations of average heat transfer of current study are depicted in Fig. 10 comparing with the experimental correlation of Al Azzawi [2] and the correlation given by Fedorov and Viskanta [35] obtained form numerical results with 20% turbulence intensity at the channel inlet. The experimental results of this study and the experimental results of Al Azzawi [2] agree perfectly in terms of trend, but with some discrepancy. Since this study and Ref. [2] are carried out using nearly identical channels, the difference between the values can be attributed to the fact that the channel used by Al Azzawi [2] had been fitted with a diffuser at the inlet to minimise disturbances. The numerical results obtained using DA model follow up the trend of experimental studies fairly well matching the experimental results of current study perfectly within the uncertainty of experimental results. The TH model overestimates average heat transfer in the complete $Ra(b/H)$ range of this study. The correlation given by Fedorov and Viskanta [35] agrees well with the experimental results of this study, However, it slightly overestimates heat transfer at lower range of $Ra(b/H)$ and under estimates at higher range. The correlating equations presented for heat transfer and induced flow rate should be used within the $Ra(b/H)$ range of 10^5 and 10^6 since present study does not have any experimental data available outside this range.

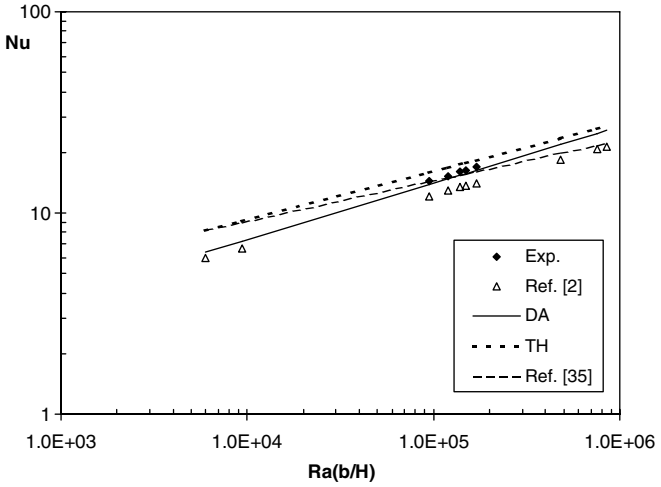

Fig. 10. Dimensionless heat transfer as function of $Ra(b/H)$.

5. Conclusions

Although laminar natural convection in vertical parallel-plate channel has been extensively studied concerning many aspects of the problem for several decades, the literature survey indicates the deficiency of experimental and theoretical work on the turbulent natural convection in vertical parallel-plate channel. The majority of existing experimental work considers uniform wall heat flux heating. The present study deals with investigation of turbulent natural convection in vertical parallel-plate channel with asymmetric heating, one wall is maintained at a uniform temperature and the opposing wall is made of glass. The study is carried out experimentally and numerically, using LDA and CFD. Three different LRN k–ε turbulence models are used in numerical calculations. Experimental and numerical velocity and turbulent kinetic energy profiles are presented along the channel at different elevations to show the flow development. Correlation equations are developed for average heat transfer and induced flow rate using numerical results. The following conclusions can be made form this study.

1. The experimental velocity profiles along the channel indicate developing character of the flow and is an important contribution to the understanding of turbulent flows in vertical parallel-plate channels.
2. Turbulent kinetic energy profiles clearly show that near the outlet fully turbulent flow is attained.
3. The experimentally determined average heat transfer data of this study have an excellent qualitative agreement with that of Al Azzawi [2]. The quantitative discrepancy may be attributed to the channel inlet geometry.
4. The numerical method along with the LRN k–ε turbulence models considered in this study are capable of predicting average heat transfer and induced flow rate almost within the limits of experimental uncertainty. The value and distribution of turbulent kinetic energy at the inlet effect predicted heat transfer and induced flow rate considerably.
5. Non of the three LRN k–ε turbulence models can be singled out as the best model for use in the present problem. Although the DA model predicts average heat transfer excellently, it cannot capture the profiles well enough qualitatively where TH model performs best.
6. Correlating equations are developed for average Nusselt and Reynolds numbers from the experimental and numerical results in terms of dimensionless parameters.
7. Additional experimental data regarding flow and temperature fields will contribute to the understanding of the problem and to the validation and evaluation of

numerical techniques. Experimental data, especially in the range of $Ra(b/h)$ below 10^5, would be very valuable for the determination of transition range from laminar to turbulent flow.

References

[1] T. Yilmaz, An experimental and numerical investigation of laminar and turbulent natural convection in vertical parallel-plate channels, PhD thesis, Department of Mechanical Engineering, University of Strathclyde, Glasgow, UK, 1997.

[2] A.R.H. Al-Azzawi, Natural convection in a vertical channel related to passive solar systems, PhD thesis, Department of Mechanical Engineering, University of Strathclyde, Glasgow, UK, 1987.

[3] D. Sohn, A numerical study of turbulent natural convection in a vertical parallel plate channel with symmetric and asymmetric heating, PhD thesis, Department of Mechanical Engineering, The Pennsylvania State University, University Park, PA, USA, 1989.

[4] D.R. Pedersen, R.R. Stewart, J.H. Tessier, J.B. Heineman, P.A. Lottes, Experimental and analytical studies of passive shutdown heat removal systems, AIChE Symp. Ser. 83 (257) (1987) 145.

[5] A. Bar-Cohen, W.M. Rohsenow, Thermally optimum spacing of vertical, natural convection cooled, parallel plates, J. Heat Transfer 106 (1984) 116–123.

[6] W. Elenbaas, Heat dissipation of parallel plates by free convection, Physica 9 (1942) 1–28.

[7] S. Ostrach, Laminar natural convection flow heat transfer of fluids with and without heat sources in channels with constant wall temperatures, NACA Technical Note, 2863, 1952.

[8] J.R. Bodoia, J.F. Osterle, The development of free convection between heated vertical plates, J. Heat Transfer 84 (1962) 40–44.

[9] R.K. Engel, W.K. Mueller, An analytical investigation of natural convection in vertical channels, ASME HT 16, Paper No. 67, 1967.

[10] W. Aung, L.S. Fletcher, V. Sernas, Developing laminar free convection between vertical flat plates with asymmetric heating, Int. J. Heat Mass Transfer 15 (1972) 2293–2308.

[11] D. Naylor, J.M. Floryan, J.D. Tarasuk, A numerical study of developing free convection between isothermal vertical plates, J. Heat Transfer 113 (1991) 620–626.

[12] E.M. Sparrow, P.A. Bahrami, Experiments on natural convection from vertical parallel plates with either open or closed edges, J. Heat Transfer 102 (1980) 221–227.

[13] Z. Li, Y. Gui, Z. Guo, Experimental investigation on the edge effect of natural convection between two vertical plates, in: R.K. Shah, E.N. Ganic, K.T. Yang (Eds.), Experimental Heat Transfer, Fluid Mechanics, and Thermodynamics, Elsevier, New York, 1988, pp. 419–424.

[14] J.R. Carpenter, D.G. Briggs, V. Sernas, Combined radiation and developing laminar free convection between vertical flat plates with asymmetric heating, J. Heat Transfer 98 (1976) 95–100.

[15] E.M. Sparrow, S. Shah, V. Sernas, Natural convection in a vertical channel: I. Interacting convection and radiation, II. The vertical plate with and without shrouding, Numer. Heat Transfer 3 (1980) 297–314.

[16] A. Moutsoglou, J.H. Rhee, J.K. Won, Natural convection–radiation cooling of a vented channel, Int. J. Heat Mass Transfer 35 (1992) 2855–2863.

[17] E.M. Sparrow, L.F.A. Azevedo, Vertical channel natural convection spanning between the fully developed limit and single-plate boundary-layer limit, Int. J. Heat Mass Transfer 28 (1985) 1847–1857.

[18] T. Burch, T. Rhodes, S. Acharya, Laminar natural convection between finitely conducting vertical plates, Int. J. Heat Mass Transfer 28 (1985) 1173–1186.

[19] S. Kim, N.K. Anand, W. Aung, Effect of wall conduction on free convection between asymmetrically heated vertical plates: uniform wall heat flux, Int. J. Heat Mass Transfer 33 (1990) 1013–1023.

[20] L.F.A. Azevedo, E.M. Sparrow, Natural convection in a vertical channel vented to the ambient through an aperture in the channel wall, Int. J. Heat Mass Transfer 29 (1986) 819–830.

[21] T. Aihara, S. Maruyama, Laminar free convective heat transfer in vertical uniform heat flux ducts (numerical solution with constant/temperature-dependent fluid properties), Heat Transfer Japanese Res 15 (1986) 69–86.

[22] E.M. Sparrow, G.M. Chrysler, L.F. Azevedo, Observed low reversals and measured-predicted Nusselt numbers for natural convection in a one-sided heated vertical channel, J. Heat Transfer 106 (1984) 325–332.

[23] W. Aung, G. Worku, Developing flow and flow reversal in a vertical channel with asymmetric wall temperatures, J. Heat Transfer 108 (1986) 299–304.

[24] E. Griffith, A.H. Davies, The transmission of heat by radiation and convection, DSIR-Br. Food Investigation Board Special Report No. 9, HMSO, London, 1922.

[25] C.Y. Warner, V.S. Arpaci, An experimental investigation of turbulent natural convection in air along a vertical heated flat plate, Int. J. Heat Mass Transfer 11 (1968) 397–406.

[26] R. Cheesewright, Turbulent natural convection from a vertical plane surface, J. Heat Transfer 90 (1968) 1–8.

[27] G.C. Vliet, C.K. Liu, An experimental study of turbulent natural convection boundary layers, J. Heat Transfer 91 (1969) 517–531.

[28] R.R. Smith, Characteristics of turbulence in free convection flow past a vertical plate, PhD thesis, Queen Mary College, University of London, London, UK, 1972.

[29] W.K. George, S.P. Capp, A theory for natural convection turbulent boundary layers next to heated vertical surfaces, Int. J. Heat Mass Transfer 22 (1979) 813–826.

[30] M. Miyamoto, Y. Katoh, J. Kurima, H. Sasaki, Turbulent free convection heat transfer from vertical parallel plates, in: C.I. Tien, V.P. Carey, J.K. Ferrel (Eds.), Heat Transfer, vol. 4, Hemisphere, Washington, DC, 1986, pp. 1593–1598.

[31] S.M. Fraser, A. Gilchrist, T. Yilmaz, Natural convection LDA measurements, in: A. Dybbs, B. Ghorashi (Eds.), Laser Anemometry Advances and Applications, ASME, New York, 1991, pp. 547–554.

[32] A. La Pica, G. Rodono, R. Volpes, An experimental investigation on natural convection of air in a vertical channel, Int. J. Heat Mass Transfer 36 (1993) 611–616.

[33] X. Cheng, U. Müller, Turbulent natural convection coupled with thermal radiation in large vertical channels with asymmetric heating, Int. J. Heat Mass Transfer 41 (1998) 1681–1691.

[34] M.A. Habib, S.A.M. Said, S.A. Ahmed, A. Asghar, Velocity characteristics of turbulent natural convection in symmetrically and asymmetrically heated vertical channels, Exp. Thermal Fluid Sci. 36 (2002) 77–87.

[35] A.G. Fedorov, R. Viskanta, Turbulent natural convection heat transfer in an asymmetrically heated, vertical parallel-plate channel, Int. J. Heat Mass Transfer 40 (1997) 3849–3860.

[36] C.K. Lam, K. Bremhorst, Modified form of k–ε model for predicting wall turbulence, J. Fluid Eng. 103 (1981) 456–460.

[37] W.M. To, J.A.C. Humphrey, Numerical simulation of buoyant turbulent flow I. Free convection along a heated vertical flat plate, Int. J. Heat Mass Transfer 29 (1986) 573–592.

[38] L. Davidson, Calculation of the turbulent buoyancy-driven flow in a rectangular cavity using an efficient solver and two different k–ε turbulence models, Numer. Heat Transfer 18 (1990) 129–147.

[39] L. Davidson, Second-order corrections of the k–ε model to account for non-isotropic effects due to buoyancy, Int. J. Heat Mass Transfer 33 (1990) 2599–2608.

[40] S.V. Patankar, Numer. Heat Transfer Fluid Flow, Hemisphere, New York, 1980.

[41] D.B. Spalding, PHOENICS Instruction Courses: Course Notes TR/300, CHAM, London, 1989.

[42] D.B. Spalding, The PHOENICS Beginners Guide TR/100, CHAM, London, 1991.

[43] J.C. Ludwig, H.Q. Qin, D.B. Spalding, The PHOENICS Reference Manual TR/200, CHAM, London, 1989.